Microstructure changes in poly(ethylene terephthalate) in thick specimens under complex biaxial loading

Yann Marco, Luc Chevalier

Polymer Engineering & Science

Microstructure changes in Poly(ethylene terephthalate) in thick specimens under complex biaxial loading

Journal:	*Polymer Engineering & Science*
Manuscript ID:	PES-07-0346.R1
Wiley - Manuscript type:	Research Article
Date Submitted by the Author:	n/a
Complete List of Authors:	Marco, Yann; ENSIETA, Laboratoire MSN Chevalier, Luc; Universite Paris-Est Marne-la-Vallee, Professeur des Universites
Keywords:	crystallization, polyesters, WAXS

Microstructure changes in Poly(ethylene terephthalate) in thick specimens under complex biaxial loading

Yann Marco[a] *, Luc Chevalier*[b,*]

[a] ENSIETA - Laboratoire MSN, 2, rue François Verny, 29806 Brest Cedex 9

[b] LaM – UPEMV, 5 boulevard Descartes, Champs sur Marne, 77454 Marne la Vallée cedex

*Corresponding author : luc.chevalier@univ-mlv.fr
Tél. 33 0(1) 60 95 77 85
Fax 33 0(1) 60 95 77 99

Acknowledgements

To EASTMANN for providing us with the PET, to G. Régnier for giving us access to samples injection and special thanks to J. Doucet for his help in the X-ray diffraction experiments.
A special thank to L. Spittal and P. Laguillaumie for their help in correcting the manuscript.

Microstructure changes in Poly(ethylene terephthalate) in thick specimens under complex biaxial loading

Yann Marco, Luc Chevalier

1 Introduction

Poly(ethylene terephthalate) is a polymer which is widely used, in its semi-cristalline state, for tensile draw, roll drawing or blow-molding processes. There are many reasons which can account for its popularity, (in particular, it presents interesting optical and barrier properties). The main one, however, is perhaps the strain hardening effect which occurs during the process, which stabilizes deformation and ensures homogeneous thickness. The microstructural changes experienced by the material (orientation, crystallization) are therefore very helpful during the processing but also improve the final product as its mechanical properties are much higher than those of the initial amorphous material. Understanding the links between the processing parameters (such as the strain ratios and rates, temperature and geometry) and the microstructural changes (during deformation and after process completion) is crucial to performing reliable optimization and numerical simulation of these processes. Ex-situ and in-situ

observations have already been achieved [1-4], giving precious information on strain-induced orientation and crystallization. Still, these previous studies were mainly based on mechanical tests with stretching in one single direction. However, due to the high anisotropy of molecular chains, the complex strain path experienced by the polymer during the industrial process, makes it more difficult to understand the micro-macro relationships.

If we focus on the blow-molding process for example, it is well known that the delay between longitudinal stretching and blowing is a crucial parameter in mastering final mechanical properties. The mechanical anisotropy induced by this process was clearly shown in a previous study [5] (Fig.1). It could seem at first glance that because of its very low thickness, the bottle would exhibit a homogeneous microstructure and that the mechanical anisotropy could be easily related to an anisotropic microstructure, induced by the sequenced path. But a closer investigation of the microstructure reveals that the WAXD pattern obtained throughout the bottle wall shows induced crystallization and yet reveals no evidence of anisotropy (Fig.1). Moreover, recent FTIR investigations [6-7] have revealed substantial orientation gradients throughout the bottle thickness.

The aim of our study is to achieve both mechanical tests representative from the blow-molding process, and micro-structural

measurements in order to link mechanical parameters to the microstructure evolutions. One difficult point in blow moulding experimental study is the need of thick specimens to be representative of the industrial preforms, which usually leads to set-up using either a blow molding machine or a close principle. The second difficult point is therefore the complex microstructure induced, which makes more difficult the understanding of the links between the mechanical history and the associated microstructure, and leads to even more complex tries to check the accuracy of numerical models. In order to obtain a more simple induced microstructure and though to be representative of the thickness of the preforms, we use here thick specimens, milled out from amorphous injected plates. These cross-shaped specimens were subjected to complex biaxial strain paths, representative of stretch blow moulding process. In order to obtain measurements both of the constitutive response during biaxial drawing and of the micro-structural evolution, we used a biaxial set-up coupled with a fast infra-red heater in order to avoid quiescent crystallization and a fast cooling-down protocol to limit crystallization kinetics during relaxation. Local strain was measured with a home-developed image correlation technique and the associated microstructure was studied by means of densimetry and WAXD. The information thus gathered made it possible to study the influence of stretching parameters and of strain type on the induced crystallization.

2 Experimental

2.1 Biaxial tests

A biaxial set-up already presented elsewhere [8, 9, 10] was customized for liquid nitrogen quenching. The biaxial tests were carried out on a triaxial testing machine named Astree (LMT-Cachan).

Figure 2 presents the different elements, including the infra-red heater, the grips and the cross-shaped specimen, the CCD camera measuring the deformation field and the quenching box. Computer monitoring and data acquisition were performed with LabVIEW®, an object-oriented application. The material was a PET designed for blow-molding application (PET 99 21 W EASTMAN) and the cross-shaped specimens were injection-molded as plates to insure that the initial microstructure would be non oriented and amorphous. The specimens were then drilled and milled. The edge radius was chosen to allow maximal elongation without local damage. The grips were designed so that only the central zone (a 50 mm side square) was heated and stretched. In order to determine the strain field, black paint was sprayed over the specimen's surface, and the time evolution of the spray pattern was monitored with a CCD camera. The evolution of the strain field could then be determined thanks to a home-developed cross correlation technique [11-12], implemented in MatlabTM. The accuracy of the method is at least on the order of 2/100th pixel and

the minimum detectable displacement is also in the order of 2/100th pixel.

Like most polymers, PET has a low thermal conductivity. Heating techniques using convection or conduction not only require a long heating time, but also lead to microstructure heterogeneity between the skin and the core of the material. An alternative is radiation heating with infrared waves, which is the usual industrial technique. The maximum variation in temperature during a test is about ±1°. Only one side of the specimen is heated, leaving the opposite side available for image acquisition with a CCD camera. Since the grips are not translucent to infrared light, only the test zone of the specimen is heated and deformed which prevents polymer shrinkage and slippage in the grips. Three types of tests were carried out at different temperatures (80, 90, 100°C) and strain rates (0.35, 0.7, 2.5, 5 s^{-1}). The first one was a true plane strain test. The second one was an equi-biaxial test in which the specimen was simultaneously stretched in the two perpendicular directions. The third one was a sequential biaxial test: the specimen is stretched firstly in one direction and then in the other one. More detailed information on these kinds of tests can be found in [10].

In order to differentiate the microstructural changes induced during the stretching from the ones that appeared during the relaxation under stress, a quenching protocol was used: a wood

box is filled very quickly with liquid nitrogen in order to freeze the microstructure. The drop in temperature of the specimen was measured and was about -180°C/second.

2 2 Morphology analysis method

In a previous work [10], we showed that PET injected specimens have no initial orientation and low initial crystallinity (less than 3%). Moreover, the study of the thermal kinetics of PET confirmed that only very low thermal induced crystallinity could develop in our tests.

WAXD experimentation was performed using a Synchrotron radiation source (LURE's beamline D43 (Orsay)). The specimens were scanned by means of a monochromated beam with a wavelength of 1,45 Å and a diameter of 0.5 mm. The distance between the sample and the detector was 80 mm. The Debye-Scherrer patterns obtained were used to determine both the chain orientation and the crystallite geometry. In the following, the unit cell we chose is the one determined by Daubeny et al [13]. Figure 3 presents a typical WAXD pattern and its associated crystalline reflections.

2.2.1 Crystallinity ratio

The crystalline ratio can be inferred from the diffraction patterns, for example from the (010) crystal reflection peak area or from a global comparison of amorphous and crystallized profiles. However, these methods turned out to be less accurate than the

density measurement technique which was the method used in this study. This technique is based on the densification occurring as the material is crystallizing. We used here a Mettler-Toledo machine to weigh the specimens in air and in water, which gives its specific mass. Using classical values used for the amorphous (d_a= 1,333 $g.cm^{-3}$ [13]) and crystalline (d_c= 1,455 $g.cm^{-3}$ [13]) phase of PET, one can therefore evaluate the crystallinity ratio. Samples were cut from zones of the stretched specimens showing no crazing, in order to limit possible uncertainties induced by micro-voids or porosity in density measurements.

2.2.2 Chains orientation

Performing a rigorous study of the chains orientation in the space would required an observation along three orthogonal directions. As the scattering vector in our study remained perpendicular to the specimen face, we could only obtain a rough approximation of the orientation function f_c. Given that benzene rings of the crystalline phase tend to lie further down in the specimen plane as strain increases and that the chains of the crystalline phase remain mainly in the plane specimen, as noted in [14], this approximation could be sufficient. Moreover, we verified in a former study [10] that orientation (measured by means of IR dichroïsm) was homogeneous along the depth of the heated and stretched specimens (this confirmed also a posteriori the temperature homogeneity obtained with the infrared heating

apparatus). In the following, we will therefore consider that a single f for the whole specimen description could give a good relative indication of the orientation in the crystalline phase. The (105) crystallographic plane, whose normal is close to the chain axis direction was investigated. The Hermann crystalline orientation function f_c was measured with azimuthal scanning of the (105) equatorial reflection (at 2θ=39.6°) whose normal is close to the chain axis direction. Background intensity was measured at the tail ends and then subtracted. The average cosine square angle $<\cos^2\phi_{105}>$ (with ϕ, the angle between the (105) plane normal and the draw direction) was calculated from the corrected azimuthal intensities $I(\phi)$:

$$<\cos^2\phi_{105}>=\frac{\int_0^{\pi/2} I(\phi).\sin\phi.\cos^2\phi.d\phi}{\int_0^{\pi/2} I(\phi).\sin\phi.d\phi} \qquad (1)$$

Moreover, let us assume that $<\cos^2\phi_{105}>$ is close to the average cosine square angle that the c-chain axis makes with the draw direction $<\cos^2\phi_c>$. The crystalline orientation derives then from the Hermann orientation relationship:

$$f_c=\frac{3<\cos^2\phi_c>-1}{2} \qquad (2)$$

The azimuthal scans were performed thanks to the Fit2D software developed by the European Synchrotron Radiation

Facility (ESRF). More details on this commonly used protocol can be found in [9].

2.2.3 Crystal morphology

The x-ray diffraction pattern makes it possible to study quantitatively the crystal lamellar morphology through a 2θ integration. The 2θ integrated profile of an amorphous specimen is subtracted from those of the stretched specimens. The profile is then deconvoluted using a curve-fitting program and peaks were analyzed as PEARSON VII curves. The crystallographic planes investigated here are mainly (1̲05) whose plane normal is close to the chain axis direction, (100) whose plane normal is close to the benzene ring normal, and (010). The reflections corresponding to these planes are pointed out in figure 3. Whenever the intensity of the reflection was too weak, we used the (1̲03) reflection plane whose normal direction is close to that of (1̲05).

The crystal size along the directions normal to these planes are then calculated using the Scherrer relationship:

$$L_{hkl} = \frac{\lambda}{\cos\theta_{hkl}.\Delta\theta_{hkl}} \qquad (3)$$

where $\Delta\theta_{hkl}$ is the angular width inferred from the deconvolution analysis. The measurement uncertainties are evaluated to 0.5 nm on the deduced crystalline lengths. Knowing the size of the crystal along three independent directions allows us to gauge its volume. If we compare the

volume of the crystals to the crystallinity ratio measured it is possible to evaluate the average number of crystals per unit volume [3].

3 Results and discussion

3.1 Mechanical results

We focus here on biaxial tension tests. Although the deformation of the specimen is obviously heterogeneous, we verified on the strain field obtained by digital image correlation that the principal elongations in the central region of the specimen were equal. The central region is in an equi-biaxial state of strain. Moreover, it is also valid to quickly evaluate the stress-strain behavior of the PET for simultaneous biaxial tension tests [15]. Figure 4 illustrates the strain hardening effect and the opposite influences of temperature and strain rate on the mechanical behavior of PET, which are well-known for uni-axial tension tests.

3.2 Crystallinity ratio

In this section, the crystallinity ratios are measured by densimetry on samples cut out from the central zone of specimens. Elongation values for the main tension directions are measured both with optical correlation technique and with a grid drawn on the samples. As in the case of uni-axial tension tests, a minimal elongation is required for crystallinity to be observed. Figure 5 illustrates this result for simultaneous biaxial and plane strain tension tests. It is worth noting that the critical elongations (about 2)

are close to the ones observed for uni-axial tension tests.

Figure 6 presents the effect of temperature on crystallinity for a given principal elongation λ, for both simultaneous biaxial and plane strain tension tests.

Similarly, figure 7 presents the effect of tension speed (the indicate value is the initial one) on the crystallinity for a given principal elongation λ, and for both simultaneous biaxial and plane strain tension tests. The sensitivity of the crystallinity ratio to the tension speed is similar for both kinds of loading, and saturates at high speed, as has already been observed for uniaxial tension tests [8]. Figure 8 compares the influence of tension speed on the crystallinity ratio (upper charts), for several draw ratios. The influence of tension speed seems to be less important for high elongations. This curve shows the same values and has the same characteristic shape observed in previous studies featuring plane strain tests on PET films [3, 16, 17, 18].

Bottom chart of figure 8 compares the crystallinity ratio evolutions with elongation for the different solicitations. The uniaxial data presented here come from tests presented elsewhere [8]. Like Chandran *et al*. [19], we have chosen here the planar extension (*i.e.* the product of the two principal elongations) to compare the different solicitations. The solicitations inducing a rapid chains orientation cause crystallization to start at a lower elongation. Moreover, for a given elongation, the crystallinity ratio is higher. It is worth noting that the

crystallinity ratio is always higher in sequential biaxial tests than in simultaneous ones. The sequential strain path seems to help the crystallization in the second stretching direction.

The values of the crystallinity ratios and the trends observed confirm the results of previous studies which used plane strain tests [3, 19, 20] and biaxial strain tests [19, 21].

The crystallinity ratios presented above are relevant for the crystals appearing during the tension and relaxation under stress phases, for specimens cooled down slowly to room temperature. A second battery of tests was carried out with the same mechanical solicitations followed by a liquid nitrogen quenching. Figure 9 compares the crystallinity ratios measured with or without quenching, for the different solicitations. Once again it appears that sequential tension tests induce a higher crystallinity ratio than simultaneous biaxial tension tests. Given that the crystallinity ratios for the quenched specimens are relatively close, the difference in the final ratios seems to be due to the phase of relaxation under stress. It therefore seems to be directly linked to the different orientations obtained at the end of the stretching phase. We observe that final orientation favors the induced crystallization by comparing plane strain test and biaxial ones (sequential or not). Moreover, crystallization kinetic depends strongly on orientation and it is therefore more difficult to limit crystallization during relaxation for the high orientations induced by plane strain and sequential biaxial tests. By comparing the differences between the crystallinity ratios for quenched

or non-quenched samples, with crystallization kinetics under orientation proposed elsewhere [22, 23], we can conclude that these two evaluations are very close.

3.2 Molecular orientation

Figure 10 gives associates a macroscopic heterogeneous displacement and deformations field with the induced microstructure measured in different zones of the specimen in the case of a simultaneous bi-axial stretching test. As expected and already shown [9], the chains are strongly oriented along the draw direction in zones 1 and 2, where the strain is almost plane. In the central zone, where the strain is nearly equi-biaxial, no preferential orientation can be seen ($f_c \approx 0$). In the diagonal region, the chains are strongly oriented in the 45° direction, which is consistent with the fact that this corresponds to a shear strain zone. The orientations measured are very close to the expected stress curves (linked to the conformation tensor) for this simultaneous stretching test. As already shown with the WAXD patterns presented in the previous section, the orientation value in the central zone of the simultaneous tension tests remains very low. Therefore, from now on, we will focus on plane strain or sequential biaxial tension tests.

A non-exhaustive evaluation of the influence of stretching parameters (draw ratio, strain rate and temperature) on the crystalline chains, in the case of plane strain case is presented in Table 1.

On figure 11, it can be observed that the chain axis aligns closer with the tension direction when the draw ratio increases. The chains

orientation value increases sharply when the draw ratio is about 3, whatever the temperature and strain rate and seems to saturate with higher draw ratios ($\lambda > 4$). It also aligns when the temperature decreases, which could be explained by a lower chain relaxation speed, and when the draw rate increases. However this parameter plays a minimal role.

These trends and the values measured are here again very close to the ones observed by Vigny *et al.* [3].

Figure 12 compares the influence of the type of solicitation on the induced crystalline chain orientation, depending on the planar extension. For sequential biaxial tests, which are balanced, we consider the final elongation and orientation, using the first stretching direction as the reference direction. The uni-axial data presented here come from tests presented elsewhere [8]. It can be observed that the induced orientation for uni-axial tension tests is typically higher than for plane strain tests. It can also be observed from figures 12 and 13 that a minimal draw ratio along the transverse axis is required so that the crystalline chains along this axis be ordered. This ratio is close to the one observed by Gohil et Salem [24]. The WAXD patterns on the right of figure 16 show that no orientation along the first stretching direction is to be observed for higher transverse draw ratios.

Several studies [23, 25, 26], for ex-situ as well as in-situ experimentation have shown that, above a critical draw ratio, the chain

orientation seems to be slightly tilted during relaxation which is confirmed by the slight deviation (around 10°) of the equatorial reflections on the WAXD patterns (see figure 10). This behavior could be explained by the strain-induced crystallization which could 'lock' the chain relaxation and by the competition between chains relaxation and crystallization kinetic, as explained with the *reptation* and *retractation* times by Mahendrasingam *et al.* [23]. Table 1 presents the crystalline orientation measured for quenched and non-quenched samples, for plane strain tension tests under several stretching conditions. It seems that the low tilt of crystalline chains is completely true for low speeds or high temperature but that a slight tilt could be seen with higher draw ratios.

Applied to the industrial case of preform blow molding, our results appear to be representative of observations made on blown bottles. Considering inner and outer radii of the preform and the final radius of the bottle, we can evaluate the orthoradial draw ratio for inner skin (λ^{T}_{inner}) and outer skin (λ^{T}_{outer}) of the bottle :

$$\lambda^{T}_{inner} = \frac{30}{8} = 3.75 \qquad \lambda^{T}_{Outer} = \frac{30}{12} = 2.5 \tag{4}$$

Considering a similar longitudinal ratio $\lambda^{L} = \frac{220}{80} = 2.75$, and taking into account the results for the microstructure induced by sequential biaxial tension testing, we can, conclude that the crystalline orientations will be completely different on the inner and outer skins. As $\lambda^{T}_{inner} > \lambda^{L}$, the crystals will be aligned along the circumference. In the

contrary, as $\lambda^{T}_{Outer} \leq \lambda^{L}$, the crystals of the outer skin are likely to be less oriented and to be aligned along the longitudinal direction. These orientations verify the measurements and trends of references [6, 7, and 27], and explain well the microstructures observed on figure 1: the WAXD analysis of the bottle will show an average isotropic and crystalline pattern, but which comes from the superposition of anisotropic patterns associated with the evolution in orientation with thickness. This remains of course a geometrical evaluation because the phenomena involved in the industrial process are much more complex, including thermal history (which is crucial as we have shown in this study) and the delay between longitudinal stretching and blowing.

3.3 Crystal morphology

In order to limit the uncertainties due to the WAXD profiles deconvolution, we will focus here on the more precise crystallographic profiles, obtained for the higher crystallinity ratios and therefore, for the higher draw ratios. The measurements give only an average value of the crystals' dimensions but give no information on their variation. The average volume and associated population per unit volume are calculated in the same way as presented in Section 2.2.3.

As we above, we study the influence of the stretching parameters on morphological data. Figure 14 presents the influence of the draw ratio for plane strain tests. A sharp increase in the crystals volume and number can be noticed for a draw ratio higher than 3. These rises are

linked to a quick growth of the crystals along the three crystalline directions. For a draw ratio higher than 3.5, the average volume reaches an upper limit and the number of crystals increases more slowly. For these elongations, the dimension along (010) remains constant and growth along the (1̲05) and (100) is moderate. The highest crystalline direction is oriented along the chain direction, which is also the stretching direction as shown in the previous paragraph. The magnitude and the trends (especially concerning the number of the crystals) are similar to Vigny *et al.'* s results [3], for close testing conditions (on films).

Table 2 presents the influence of the temperature for a high draw ratio ($\lambda \approx 4$) and low initial draw rate (0.35 s^{-1}) in plane strain tests. The number of crystals decreases when temperature rises and the average volume shows a peak at 90°C. This variation is mostly due to the variation in crystals dimension along the chain axis. The influence of the draw rate is shown in figure 15, for a given temperature and draw ratio. It can be observed that the average volume increases with the draw rate, which implies that the number of crystal decreases, bearing in mind that the crystallinity ratios does not depend much on draw rate. It is also worth noting that the draw rate influences mainly the crystals' dimension along the chain axis, with hardly any influence on the other dimensions. Therefore, for a given draw ratio, the draw rate significantly increases the crystallites' anisotropy.

If we consider now in figure 16 the evolution in crystal

morphology induced by simultaneous biaxial tension tests, we observe here again that the average volume of the crystals decreases when the draw rate rises and that the number of crystals remains stable and decreases for the highest draw rates. The crystals' dimensions remain quite similar, showing a moderate growth along the (105) and (100) directions. The number of crystallites that appear during simultaneous biaxial tension tests are of the same magnitude than those which appear during plane strain tension tests. However, the crystals exhibit lower anisotropy and are smaller, whatever the tension speed. These observations stem from a comparison between two tests with different draw ratios but could also be observed on figure 17 for similar draw ratios.

Figure 17 also gives information on sequenced strain path and on quenching. Firstly, we will analyze the influence of the quenching process: (i) the volume of crystals is always smaller for the quenched samples, which indicates that crystallization continues during relaxation; (ii) this crystallization is mostly due to crystal growth along the (100) and (-105) directions, since the number of crystals is constant and hence no germination occurred; (iii) the number of the crystals is even decreases during plane strain tests for the two tension speeds considered. This could be explained by uncertainties in measurements but also by a « welding » of the crystals during the relaxation, favored by their very high orientation; (iv) in the case of plane strain tests and for quenched samples, anisotropy is only visible at high tension speeds. This could

either be due to growth during stretching but also to the very quick growth induced by the orientation during relaxation which makes a perfect quench difficult to perform; (v) the smallest crystalline dimension is measured along the (100) direction. It increases during the relaxation.

If we now compare the morphologies measured for the different solicitations, we can conclude that: (i) simultaneous biaxial tension tests lead to lower crystal volume than sequential biaxial tension tests. The latter itself is lower than the ones induced by plane strain tension tests, for quenched or non-quenched samples; (ii) the difference between the volumes measured increases mainly during the relaxation phase, which is probably due to the differences in crystalline chain orientation. This hypothesis is confirmed by the influence of tension speed on crystal volume observed during plane strain tests. (iii) the crystals created by a sequential tension test are more anisotropic than the ones observed after simultaneous tension tests. Considering the quenched samples, we can also observe that the number and size of crystals along the chain axis are very close to the ones observed after plane strain tension tests. We can therefore suppose that the crystals created during the first stretching phase have rotated and not broken during transverse stretching.

4. Conclusion

The several biaxial tension tests we have carried out yield many results on the evolution of PET microstructure for various multiaxial loads

(types, draw rates and draw ratios, temperature) in thick samples, which have rarely been described. The quenching set-up allows precious evaluation of the microstructure evolution after stretching. The influence of the stretching parameters on the microstructure can be observed in the quenched samples. They modify mainly the number of the crystals, *i.e.* the germination phase. However, as in the case of uni-axial solicitations [8], we have observed that the crystallization occurs mainly during relaxation. We can therefore explain the major influence of chains orientation at the end of the solicitation. The higher the orientation induced by stretching parameters or/and solicitation type the higher the crystals' volume and anisotropy and the higher the crystalinity ratio. The orientation of the crystalline phase is strongly related to the stress tensor, as well shown by the comparison between the macroscopic strains field and the local crystalline orientations. The accuracy of the optical measurement has shown that a slight difference between the elongations is enough to induce some chains orientation. We have also demonstrated that crystalline orientation does not change much during relaxation, which could be explained by the competition between molecular relaxation and crystalline growth, which « locks » chain orientation. If we focus on sequential biaxial tension test, we observed a critical transverse elongation before the re-orientation of the crystals. This re-orientation seems to come from partial breaks (fewer crystals, lower volume) but also and mainly from a rotation of crystals created during the first stretching. The sequential strain path induces higher

crystallinity and crystal orientation than the simultaneous tension tests.

Applied to the industrial case of preform blow molding, our results appear to be representative and helpful in order to understand the microstructural observations made on blown bottles.

References

[1] Casey M, *Polymer* **18** (1977)

[2] Cakmak M, Spruiell JE, White JL and Lin JS, *Polymer Engineering and Science* **27** 12 (1987)

[3] Vigny M, Tassin JF, Gibaud A, Lorentz G, *Polymer Engineering and science* **37** (1997)

[4] Mahendrasingam A, Martin C, Fuller W, Blundell, MacKerron DH, Oldman J, Harvie JL, Riekel RC, Engström P, *Polymer,* **40** (1999)

[5] Chevalier L, *Rubber and Composite Processing and Application* **28** (1999)

[6] Everall N, MacKerron D, Winter D, *Polymer* **43** (2002)

[7] Matthew R. Smith, Sharon J. Cooper, Derek J. Winter, Neil Everall, *Polymer* **47** (2006)

[8] Marco Y. Ph D Thesis of ENS de Cachan (2003)

[9] Marco Y, Chevalier L, Chaouche M, *Polymer* **43** (2002)

[10] Marco Y, Chevalier L, Régnier G, Poitou G, *Macromolecular Symposia* **185** (2002)

[11] Chevalier L, Calloch S, Hild F, Marco Y, *Eur. J. Mech. A/solids* **20** (2001)

[12] Hild F, Roux S, *CRAS Mecanique* **334** 1 (2006)

[13] Daubeny RP, Bunn CW, Brown CJ. *Proc R Soc London* **A 226** (1954)

[14] Göshel U, Deutscher K, Abetz V. *Polymer* **31** 1 (1996)

[15] Chevalier L, Marco Y, *Mechanics of Materials* **39** 6 (2007)

[16] Le Bourvellec G, Monnerie L, Jarry JP, *Polymer* **27** (1986)

[17] Ajji A, Cole KC, Dumoulin MM, Brisson J, *Polymer* **36** (1995)

[18] Salem DR, *Polymer* **33** 15 (1992)

[19] Chandran P, Jabarin S, *Advances in Polymer Technology* **12** 2 (1993)

[20] Faisant de Champchesnel JB, Tassin JF, Monnerie L, Sergot P, Lorentz G, *Polymer* **38** 16 (1997)

[21] Adams AM, Buckley CP, Jones DP, *Polymer* **41** (2000)

[22] Blundell DJ, MacKerron DH, Fuller W, Mahendrasingam A, Martin C, Oldman RJ, Rule RJ, Riekel C, *Polymer* **37** (1996)

[23] Mahendrasingam A, Blundell DJ, Martin C, Fuller W, MacKerron DH, Harvie JL, Oldman RJ, Riekel RC. *Polymer* **41** (2000)

[24] Gohil RM, Salem DR, *J. App. Polym. Sci.* **47** (1993)

[25] Gorlier E, Haudin JM, Billon N. *Polymer* **42** (2001)

[26] Matthews RG, Ajji A, Dumoulin MM, Prud'homme RE. *Polymer* **41** (2000)

[27] Gorlier E, Ph D Thesis of Ecole Nationale Supérieure des Mines de Paris (2001)

Table captions

Table 1: Evolution of the orientation function of the crystalline chains with elongation, for plane strain tests: influence of the initial draw rate, temperature and quenching protocol for a final elongation of 4.

Table 2: Influence of the temperature on the average crystal volume and crystals volumic density. Measurements achieved on plane strain tested specimens (elongation = 4, initial draw rate = 0.35 s^{-1}). Influence of temperature on crystal lengths. Measurements performed on plane strain tested specimens (elongation = 4, initial draw rate = 0.35 s^{-1}).

Figure captions

Figure 1: Illustration of the mechanical anisotropy induced by the blow molding process and pictures of transmission WAXD associated to the initial preform (left) and final bottle (right).

Figure 2: Astree triaxial testing machine, biaxial specimens geometry, biaxial testing apparatus including IR heater, CCD camera for the displacement field acquisition and liquid nitrogen quenching.

Figure 3: Typical WAXD pattern for PET, showing crystal reflections.

Figures 4: Stress versus elongation curves for PET under simultaneous biaxial tension tests, for several temperatures and tension speeds.

Figures 5: WAXD patterns showing the influence of elongation during simultaneous biaxial tests (upper left) and plane strain (upper right) for identical stretching parameters (90°C, initial draw rate = 0.35 s^{-1}). Crystallinity ratio measurements showing the influence of the elongation during simultaneous biaxial tests (lower left) and plane strain (lower right) for identical stretching parameters (90°C, initial draw rate = 0.35 s^{-1}).

Figure 6: WAXD patterns showing the influence of the temperature during simultaneous biaxial tests (upper left) and plane strain (upper right) for identical stretching parameters (elongation = 3, initial draw rate = 0.35 s^{-1}). Crystallinity ratio measurements showing the influence of the temperature during simultaneous biaxial tests (lower left) and plane strain (lower right) for identical stretching parameters (elongation = 3, initial draw rate = 0.35 s^{-1}).

Figure 7: WAXD patterns showing the influence of the initial draw rate during simultaneous biaxial tests (upper left) and plane strain (upper right) for identical stretching parameters (elongation = 3, 90°C). Crystallinity ratio measurements showing the influence of the initial draw rate during simultaneous biaxial tests (lower left) and plane strain (lower right) for identical stretching parameters (elongation = 3, 90°C).

Figure 8: Evolution of the crystallinity ratio depending on the elongation for several initial draw rates (temperature = 90°C). Results are presented for simultaneous biaxial tests (upper left) and plane strain (upper right). Evolution of the crystallinity ratio with planar extension for different mechanical paths and identical stretching parameters (90°C, initial draw rate = 0.35 s^{-1}).

Figure 9: Crystallinity ratio measurements showing the influence of nitrogen quenching for different mechanical paths and identical stretching parameters (Elongation = 4, 90°C, initial draw rate = 0.35 s^{-1}).

Figure 10: Association of measured WAXD patterns with elongation, crystallinity ratio and orientation measurement, for different zones of a simultaneously and biaxial stretched specimen (100°C, 100 mm/s).

Figure 11: Evolution of the orientation function of the crystalline chains with elongation, for plane strain tests, achieved for 90°C and 100°C (initial draw rate of 0.35 s^{-1}).

Figure 12: Evolution of the orientation function of the crystalline chains with planar extension for different mechanical paths and identical stretching parameters (90°C, initial draw rate = 0.35 s^{-1}).

Figure 13: WAXD patterns showing the differences between simultaneous and sequenced biaxially stretched specimens and the importance of transverse draw ratio on the crystalline orientation.

Figure 14: Influence of elongation on the crystals' morphological parameters: average crystal volume and crystal volumic density (left); crystal dimensions (right). Measurements performed on plane strain tested specimens (90°C, initial draw rate = 0.35 s^{-1}).

Figure 15: Influence of the initial draw rate on crystals' morphological parameters: average crystal volume and crystals volumic density (left); crystal lengths (right). Measurements performed on plane strain tested specimens (90°C, elongation = 4).

Figure 16: Influence of the initial draw rate on the crystals' morphological parameters: average crystal volume and crystal volumic density (upper left); crystal dimensions (upper right). Measurements performed on simultaneously and sequenced biaxially stretched specimens (90°C, elongation = 4). Evolution of the crystal volumic density (lower left) and average crystal volume (lower right) for different mechanical paths and draw rates. Other stretching parameters are identical (90°C, elongation = 4).

Figure 17: Evolution of the crystal dimensions for different mechanical paths and draw rates. Other stretching parameters are identical (90°C, elongation = 4).

Plain strain tests parameters			Orientation function (-105)	
Elongation λ	Temperature (°C)	Initial strain rate (s^{-1})	Not quenched	Nitrogen quenched
4	80	0.35	0.73	-
4	90	0.35	0.69	0.7
4	90	0.7	0.73	-
4	90	2.5	0.75	0.81
4	90	5	0.71	-
4	100	0.35	0.65	0.64

Table 1

	Plain strain tests ; λ=4 ; Initial strain rate =0.35 s-1		
Temperature (°C)	80	90	100
Crystal length along (010) (Å)	21	39	39
Crystal length along (100) (Å)	44	44	43
Crystal length along (-105) (Å)	28	76	45
Average crystal volume (X 10^{-25} m^3)	0,35	1,36	0,83
Crystal volumic number (X 10^{25} m^{-3})	0,88	0,27	0,26

Table 2

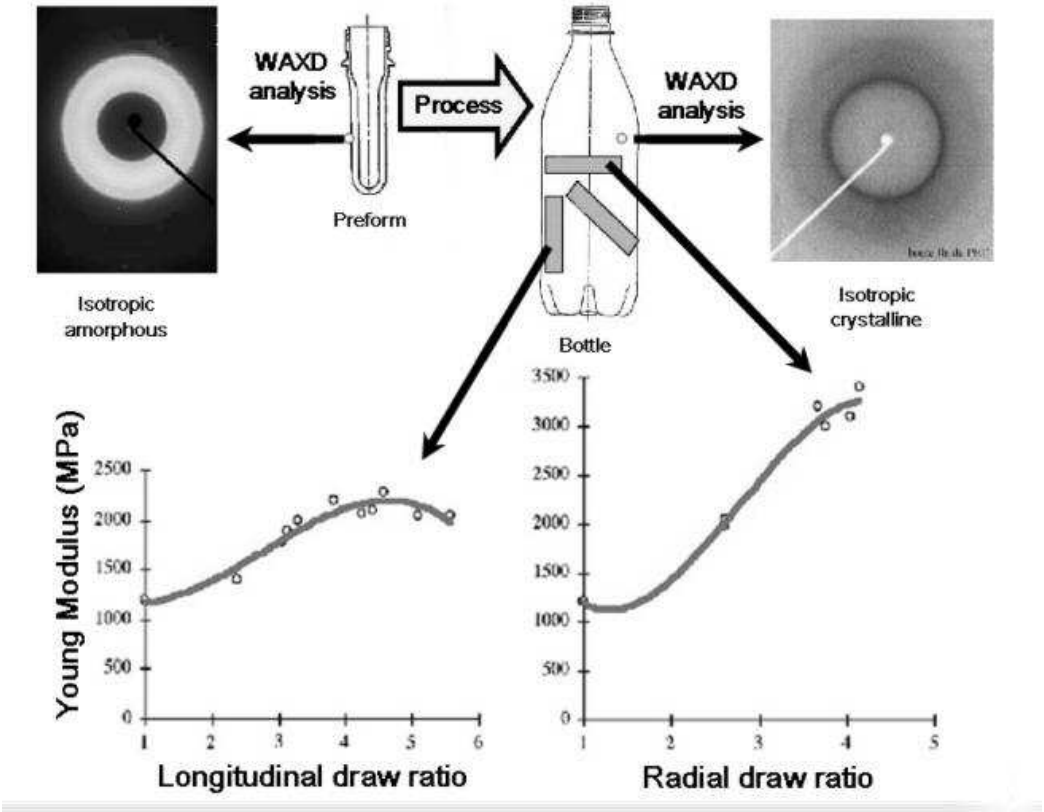

Figure1

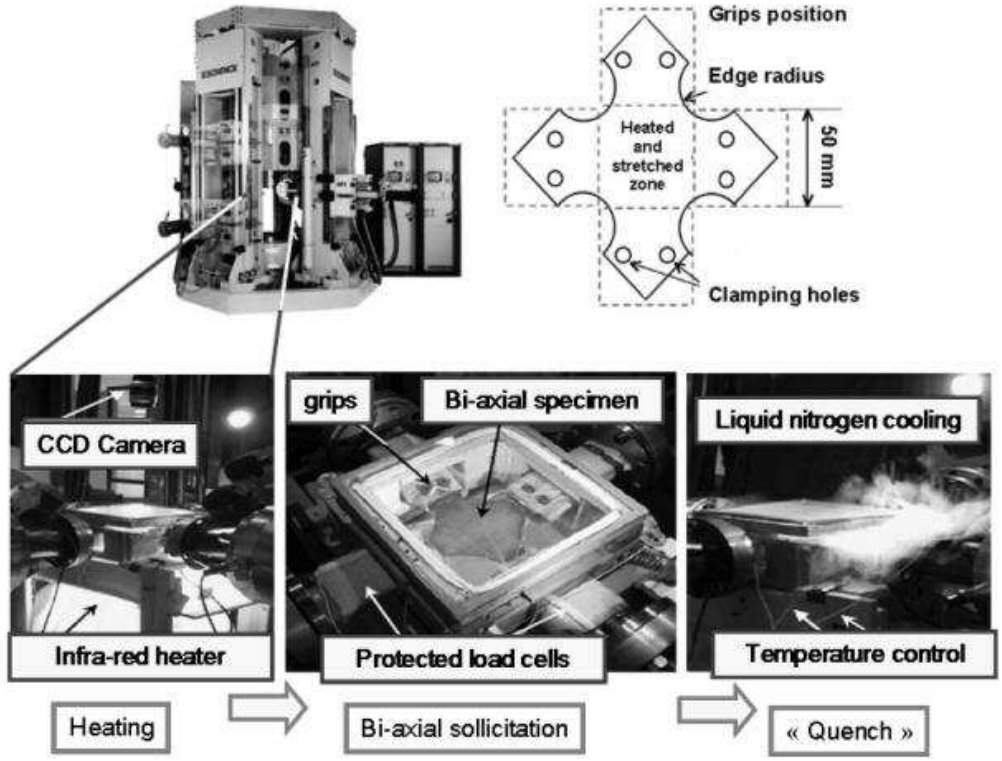

Figure 2

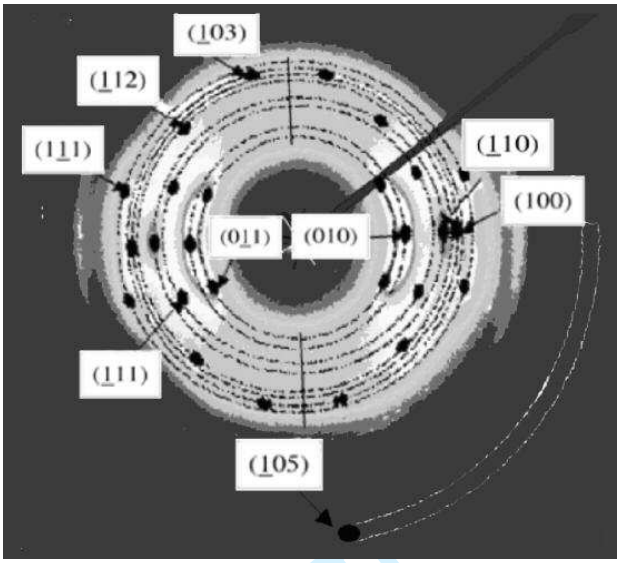

Figure 3

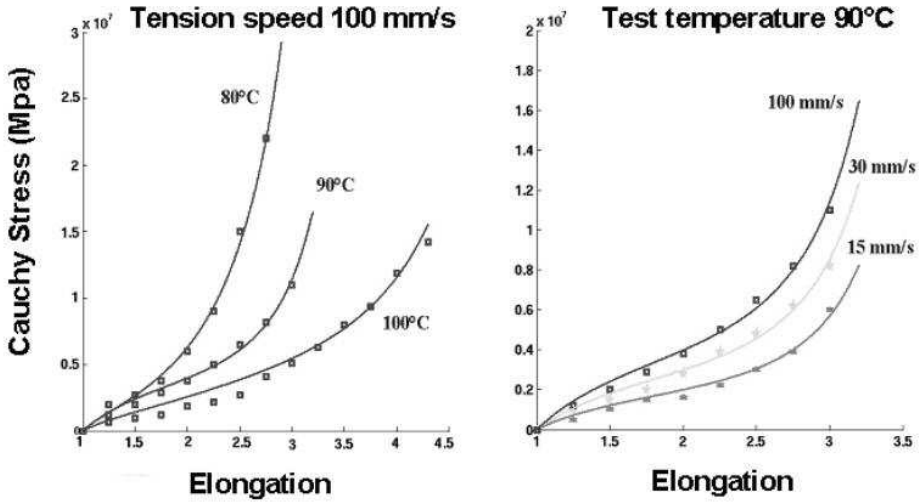

Figure 4

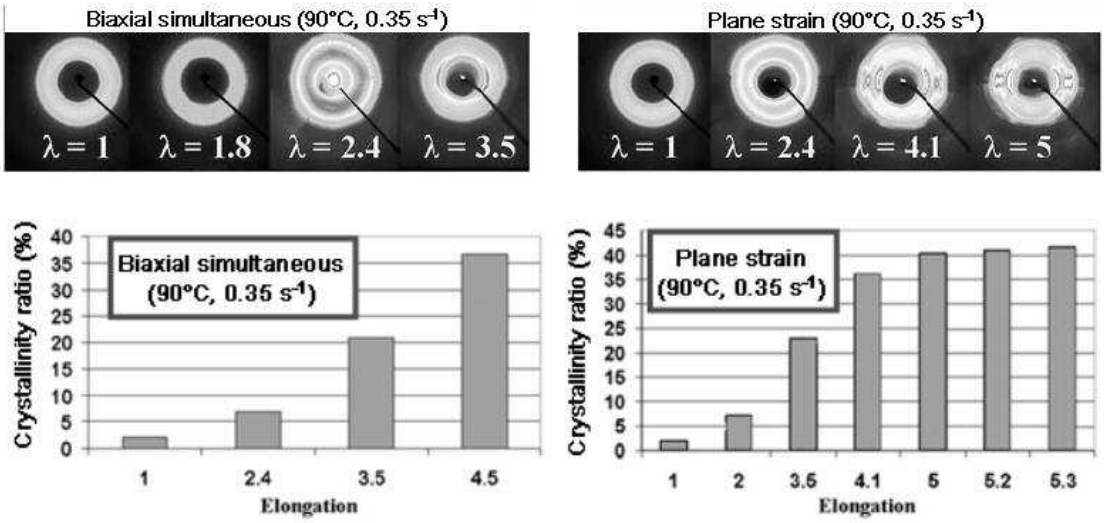

Figure 5

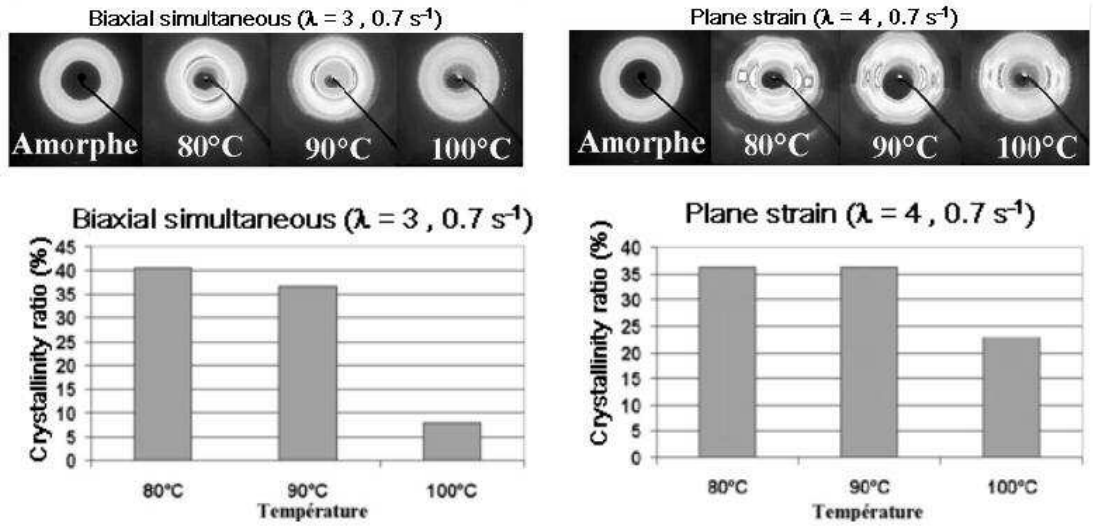

Figure 6

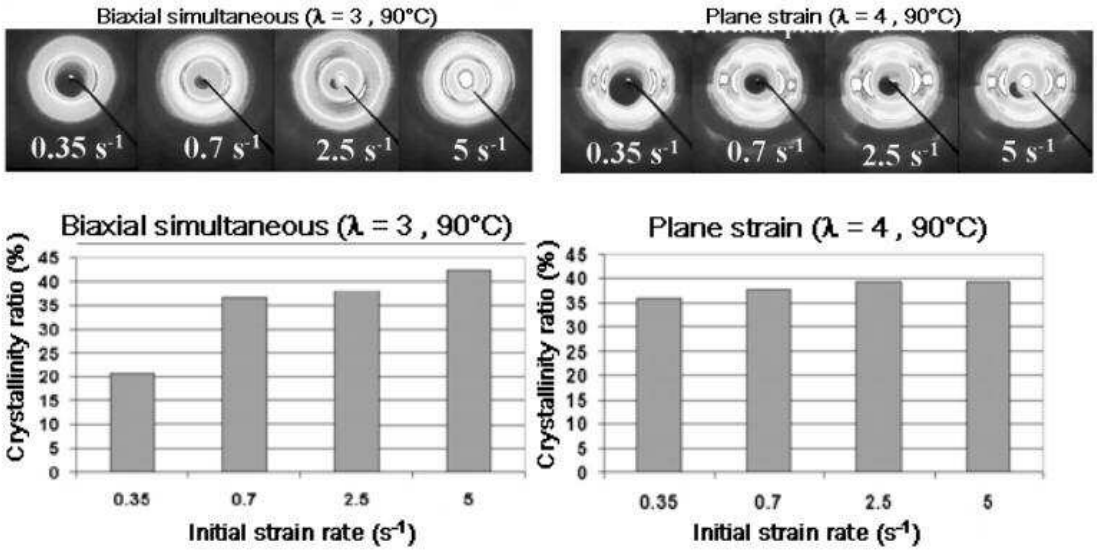

Figure 7

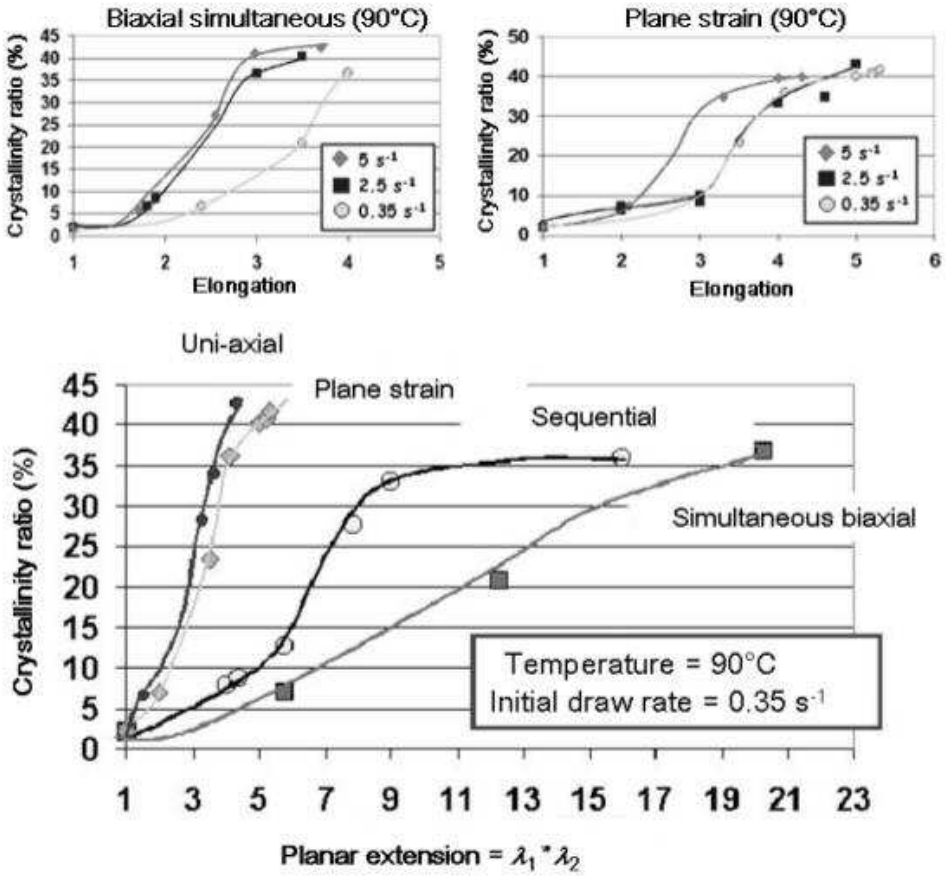

Figure 8

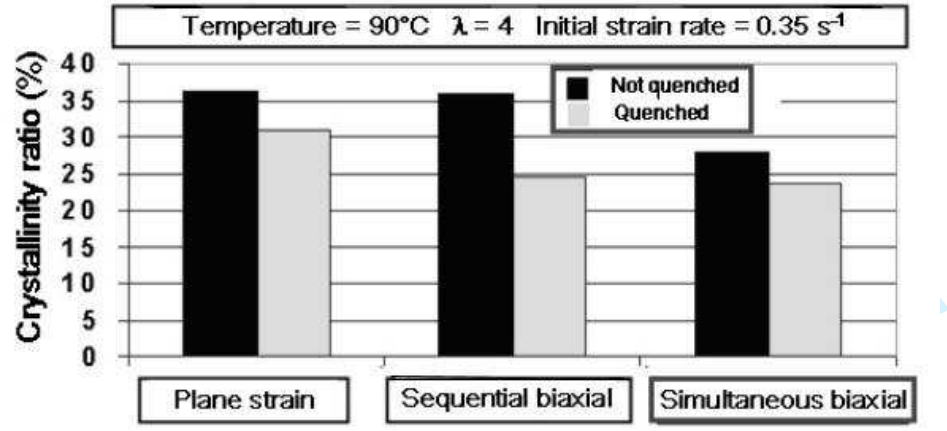

Figure 9

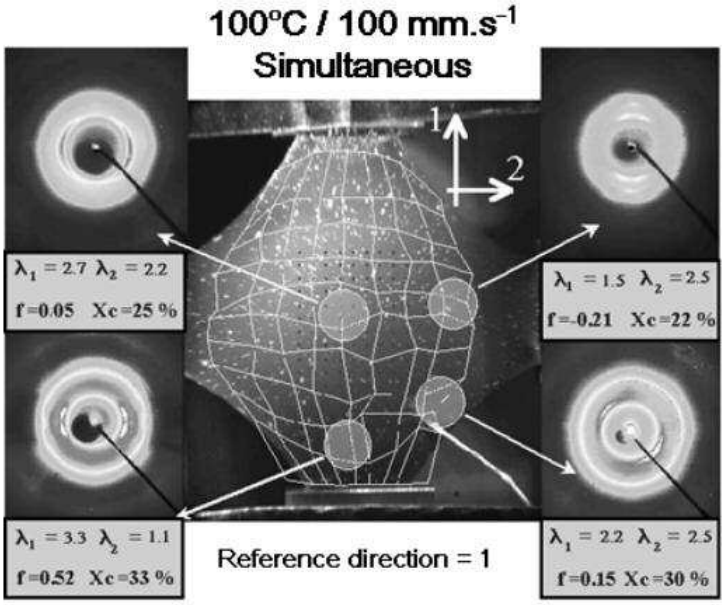

Figure 10

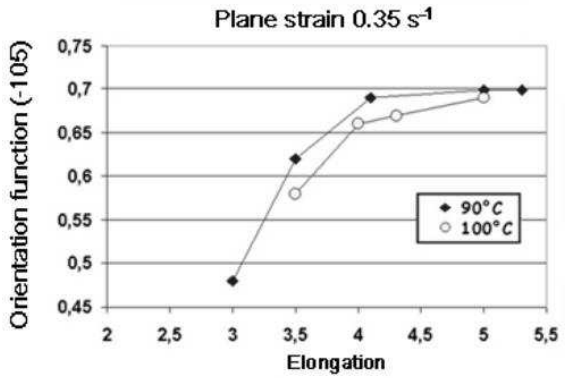

Figure 11

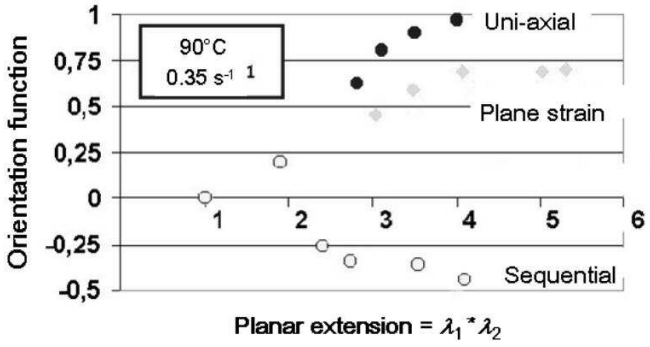

Figure 12

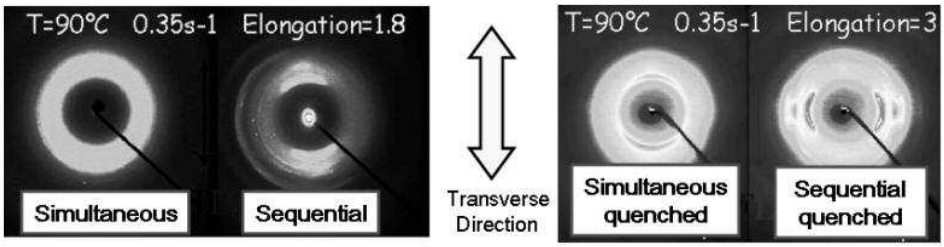

Figure 13

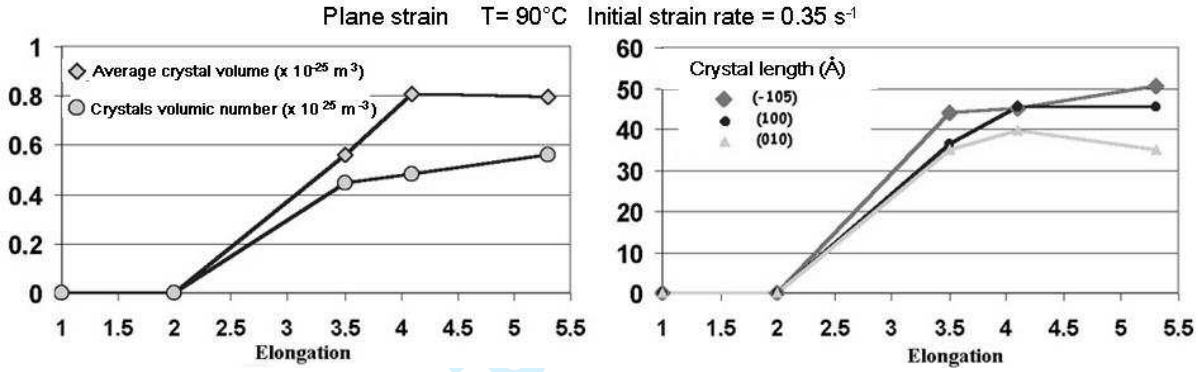

Figure 14

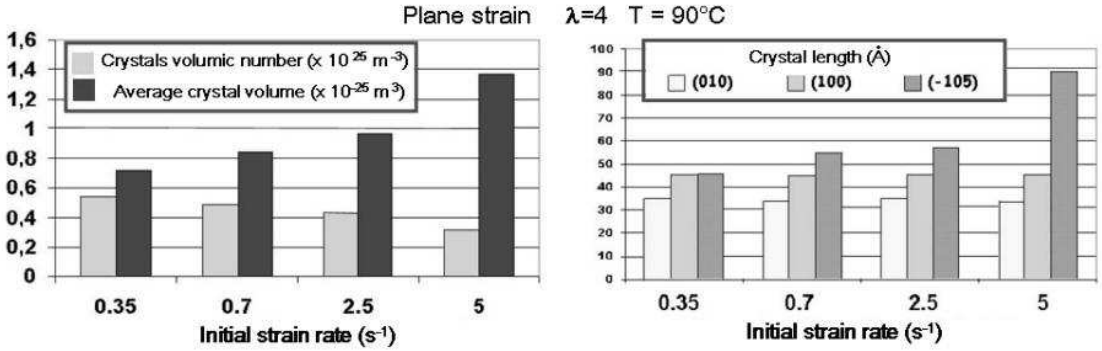

Figure 15

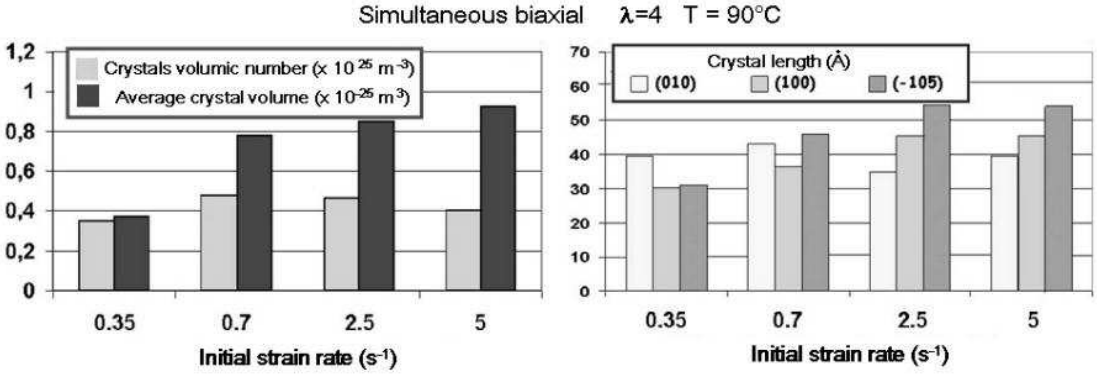

Figure 16

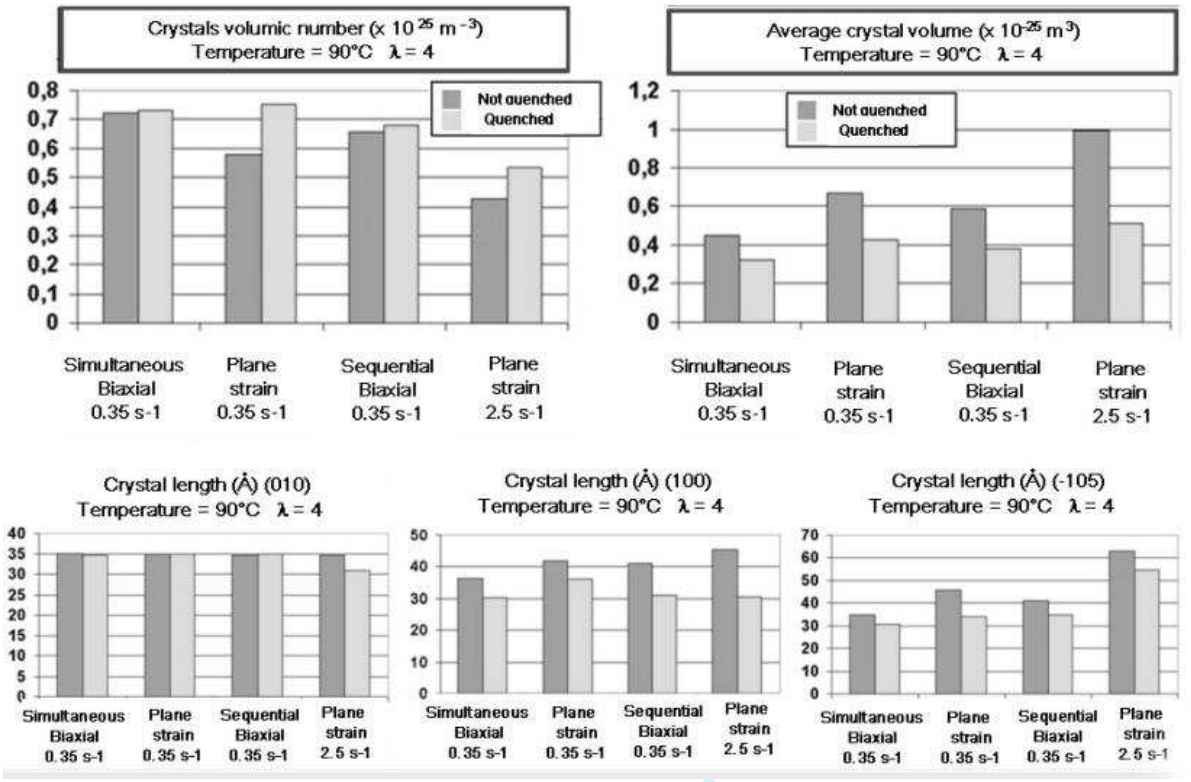

Figure 17